

First-principles calculations of the electronic and optical properties of penta-graphene monolayer: study of many-body effects

Babak Minaie ^{a,*}, Seyed A. Ketabi ^{a,*}, José M. De Sousa ^{b,*}

^a*School of Physics, Damghan University, Damghan, Iran*

^b*Instituto Federal de Educação, Ciência e Tecnologia do Piauí – IFPI, Primavera, São Raimundo Nonato, 64770-000, Piauí, Brazil.*

Abstract

In the present work, first-principles calculations based on the density functional theory (DFT), GW approximation and Bethe–Salpeter equation (BSE) are performed to study the electronic and optical properties of penta-graphene (PG) monolayer. The results indicated that PG is a semiconductor with an indirect band gap of approximately 2.32 eV at the DFT-GGA level. We found that the utilization of the GW approximation based on many-body perturbation theory led to an increase in the band gap, resulting in a quasi-direct gap of 5.35 eV. Additionally, we employed the $G_0W_0 - RPA$ and $G_0W_0 - BSE$ approximations to calculate the optical spectra in the absence and in the presence of electron-hole interaction, respectively. The results demonstrated that the inclusion of electron-hole interaction caused a red-shift of the absorption spectrum towards lower energies compared to the spectrum obtained from the $G_0W_0 - RPA$ approximation. With the electron-hole interaction, it is found that the optical absorption spectra are dominated by the first bound exciton with a significant binding energy 3.07 eV. The study concluded that the PG monolayer, with a wider band gap and enhanced excitonic effects, holds promise as a suitable candidate for the design and fabrication of optoelectronic components.

Keywords: Penta-graphene, Bethe-Salpeter equation, GW approximation, Exciton

1. 1. Introduction

Carbon atom is capable of forming various allotropes at different dimensions due to its unique electron configuration. Graphite, diamond, fullerenes [1], carbon nanotubes [2], graphene, and graphyne [3] are among the carbon allotropes. Each of these allotropes possesses unique and distinct properties compared to the others. The successful synthesis of graphene [4] has led to a great interest in the investigation of graphene-based nanomaterials among many researchers. Graphene, due to its two-dimensional structure and extremely low thickness (approximately the diameter of a carbon atom), as well as its unique properties

*Corresponding authors: babminaie@std.du.ac.ir (Babak Minaie) and saketabi@du.ac.ir (Seyed Ahmad Ketabi) and josemoreiradesousa@ifpi.edu.br (José M. De Sousa)

such as high carrier mobility, thermal conductivity, and mechanical stability, holds great potential for various industrial applications [5, 6, 7, 8, 9, 10, 11].

However, despite the mentioned features, graphene is a zero-bandgap semiconductor, which significantly hinders its direct application in optoelectronic-based devices. It is notable that the structure-property relationship is an important fundamental research issue in the field of 2D materials. Therefore, extensive theoretical and experimental studies have been conducted to modify the bandgap of graphene [12, 13, 14, 15, 16]. Various methods have been proposed to induce a bandgap in the graphene structure, such as applying an electric field, strain, chemical functionalization and doping processes. Another approach to modify the structural properties is the logical manipulation of the blocks that form the desired structure, which can lead to a new class of materials with improved characteristics. As a result, significant efforts have been devoted to the search for suitable geometrical blocks beyond the conventional hexagonal ones. The design and synthesis of pentagonal materials heavily rely on flexibility in bonding and hybridization of elements. Carbon has emerged as the researchers first choice for this purpose due to its ability to form single, double, and triple bonds and exhibit various hybridizations, including sp , sp^2 and sp^3 . Furthermore, the successful isolation of C_{20} fullerene, which consists solely of 12 pentagons [17], has expanded the availability of other low-dimensional pentagonal materials.

Based on extensive computational simulations, in 2015, penta-graphene (PG), a 2D carbon allotrope composed exclusively of pentagonal blocks, was proposed [18] and subsequently, extensive studies on PG and its derived structures have been conducted [19, 20, 21]. Some previous studies have investigated the thermal transport properties [22], optical properties [23], and mechanical properties [24] of PG, as well as its electronic properties using approaches such as tight-binding model and DFT-GW methods [25]. In a study conducted by Li et al. [21], utilizing the VASP computational package and employing the generalized gradient approximation (*GGA*) with the inclusion of Perdew-Burke-Ernzerhof (*PBE*) and the Heyd-Scuseria-Ernzerhof (*HSE06*) functionals, it was demonstrated that chemical functionalization, specifically hydrogenation and fluorination, can effectively modify the mechanical and electronic properties of PG. Their studies demonstrate that chemical functionalization increases the band gap of PG and, in particular, brings its semiconductor nature closer to insulators. In a similar work, Jia et al. [26] using first-principles calculations based on DFT, investigated the electronic, mechanical, and piezoelectric properties of hydrogen- and fluorine-functionalized PG sheets. Their calculations demonstrate that the band gap of the PGsheet increases from 3.25 eV to 4.86 eV, 4.6 eV and 4.42 eV upon hydrogenation, hydro- fluorination, and fluorination of the structure, respectively. In addition to chemical functionalization, the use of different approximations and functionals for calculating the properties of PG can lead to different results. Zhi Gen et al. [20] investigated the electronic properties of monolayer PG and compared the results with multilayer PG using the HSE06 and *optB88 - vdW* functionals. Their results showed that the calculated band gap using the *HSE06* functional for PG with different layer numbers are all direct, and increasing the number of layers did not change the gap from direct to indirect. Einolazadeh et al. [27] studied the electronic properties of PG sheet in DFT-LDA level and also GW-level.

Their calculations demonstrated that the inclusion of electron-electron interactions

through the *G0W0* approximation leads to an increased band gap. Unlike graphene, which has been extensively studied to discover its various properties, and it can be said that research related to it is almost saturated, the studying on PG structures are still at an early stage. Furthermore, most previous studies have focused on the obtaining the ground state properties of this structure, and the investigation of excited states and the properties of the structure under many-body interactions, especially electron-hole interactions, has been overlooked. Therefore, in this work, we intend to investigate the electronic and optical properties of the PG monolayer by combining DFT with the GW approximation and solving the Bethe-Salpeter equation. To achieve this, we will first calculate the ground state properties of the structure using density functional theory and then by considering the screened Coulomb electron-electron interaction through the GW approximation and solving the Dyson equation, we will obtain the quasi-particle energies. Finally, by taking into account the electron-hole interaction and solving the Bethe-Salpeter equation, we will examine the effects of excitons on the band structure and optical spectra of the PG monolayer. The description of the computational schemes is introduced in Section 2. The results and discussion are presented in Section 3, followed by conclusions in Section 4.

2. Computational Methodology

In this section, we present the computational methods based on which we performed our calculations to investigate the electronic and optical properties of PG. In the first step, for structural optimization and electronic-band structure calculations of PG monolayer, first principle calculations were performed in the framework of DFT as implemented in the QUANTUM-ESPRESSO computational package. The PBE [28, 29] functional of generalized gradient approximation (GGA) [30] was adopted to describe electron exchange-correlation.

Furthermore, the Martin-Taylor pseudopotential [31] which is of norm-conserving type was employed to investigate the electron-ion interactions. To ensure accurate and minimally error-prone calculations, an optimal number of k-points of $14 \times 14 \times 1$ were chosen in the primitive unit cell of the PG monolayer. The convergence threshold for the total energy was set to around 10^{-4} eV/atom, and the force convergence threshold was set to around 10^{-5} eV/Å. A suitable energy cutoff of 50 Ry was considered for this structure. According to the value of the bond lengths of $C_1 - C_1$ (1.550 Å) and $C_2 - C_2$ (1.329 Å), a vacuum distance of 15 Å in the perpendicular direction is considered to avoid interactions with adjacent periodic structures. It should be noted that DFT is only capable of calculating the ground state properties of the system and has limitations in determining excited states. However, to calculate the band structure and obtain the band gap of a system, we need at least one electron in the conduction band, which itself is an excited state. Therefore, we need to go beyond density functional theory. The GW approximation in the framework of many-body perturbation theory is based on the Green's function formalism and quasi-particle concept [32].

The results obtained from the GW approximation for calculating the band gap of a many-body system show good agreement with available experimental results [33] [33]. Therefore, in the next steps, we also use the GW approximation to calculate and determine the electronic

properties of excited states. In order to study the quasi-particle energies within the many-body perturbation theory, the exchange-correlation potential employed by DFT must be replaced by the self-energy operator calculated within the GW approximation [34] on the basis of the generalized Plasmon-pole Model [35]. The self-energy Σ has been calculated as the product of one-electron Green's function G_0 and the screened coulomb potential W_0 , i.e., $\Sigma = iG_0W_0$. To obtain the optical properties of a structure, the behavior of various optical quantities as a function of incident photon energy needs to be studied. Calculating the dielectric function, which is a function consisting of both real and imaginary components, serves as a starting point for describing the optical properties of a structure. Therefore, we intend to calculate the dielectric function for PG monolayer using the following two approaches:

- The random phase approximation based on the quasi-particle energies, where only screened Coulomb interactions between electrons are considered ($G_0W_0 - RPA$).
- Solving the Bethe-Salpeter equation (BSE) based on the two-particle Green's function, where in addition to electron-electron interactions, electron-hole interactions are also taken into account ($G_0W_0 - BSE$).

To solve the Bethe-Salpeter equation, we use the following relation [36, 37],

$$(E_{ck}^{qp} - E_{vk}^{qp})A_{vck}^s + \sum_{k'v'c'} \langle vck | K^{eh} | v'c'k' \rangle A_{v'c'k'}^s = \Omega^s A_{vck}^s, \quad (1)$$

where E_{ck}^{qp} and E_{vk}^{qp} denote the quasi-particle energies of conduction and bands at the specific wave vector, respectively. K^{eh} is the electron-hole screened interaction kernel. A_{vck}^s and Ω^s are the exciton eigenvalue, respectively. $|vck\rangle$ and $|v'c'k'\rangle$ denote the quasi-electron and the quasi-hole states, respectively. The calculations performed using the YAMBO [38] computational code.

3. Results and discussion

This Section presents the results of the calculations based on the formalism described in Section 2. To continue, in the following subsections, we study the dynamical stability, the electronic and optical properties of the PG monolayer, such as phonon dispersion, electronic band structure, dielectric function and the other optical parameters.

3.1. Phonon Dispersion and Dynamical Stability

Figs. 1(a) and 1(b) show schematically the top view and side view of the buckled PG monolayer structure, respectively. After optimizing the structure using the QUANTUM-ESPRESSO computational code, the lattice constant was obtained as $a = 3.64 \text{ \AA}$, which is in perfect agreement with other results [18]. The unit cell of the PG monolayer structure

consists of 6 carbon atoms with sp^2 and sp^3 hybridizations is shown in Fig. 1a, where C_1 atoms have sp^3 hybridization and C_2 atoms have sp^2 hybridization.

The bond length between $C_1 - C_1$ atoms and $C_2 - C_2$ atoms were obtained 1.550 Å and 1.329 Å, respectively. The thickness of the buckled structure or the buckling height is calculated to be $h = 1.2$ Å. Such buckling can also be seen in other mono-atomic monolayer crystals such as silicene, germanene, stanene and black phosphorus. To determine the dynamical stability of PG monolayer structure, the phonon spectrum of the structure needs to be calculated. Panel (a) in Fig. 2 illustrates the phonon dispersion curves and the corresponding phonon density of states for the PG monolayer along the high-symmetry points of the first Brillouin zone. Based on the phonon spectrum, it can be inferred that the structure is stable since there are no negative phonon frequencies, indicating the absence of imaginary phonon modes throughout the first Brillouin zone. According to the phonon spectrum of PG, there are three acoustic branches, two of which are longitudinal (L) and transverse (T) modes within the plane, and the other is an out-of-plane (Z) mode. In the vicinity of the Γ point, the scattering of the two acoustic modes (TA and LA) is linear, while the scattering of the out-of-plane mode (ZA) is quadratic (q_2). Furthermore, based on the phonon density of states shown in panel (b), it can be observed that the C_2 atoms with sp^2 hybridization have the highest contribution to the formation of optical phonons, where the highest phonon density of states associated with the vibrations of C_2 atoms is approximately at a frequency of 1600 cm^{-1} . The results obtained for the calculations related to the PG phonon spectrum are in good agreement with the results of the others [23].

3.2. Electronic Properties

To investigate the electronic properties of PG monolayer, we calculated its band structure using two approximations, LDA and GGA-PBE, at the DFT level, and the GGA-PBE approximation at the G_0W_0 level along high-symmetry k -points. Panel (a) in Fig. 3 shows the band structure of PG in the GGA-PBE approximation. The Fermi energy is considered at the zero point and the coordinates of the high-symmetry k -points at $\Gamma(0, 0, 0)$, $X(0.5, 0, 0)$, and $M(0.5, 0.5, 0)$.

As observed, in the DFT-GGA level, PG monolayer is a semiconductor with an indirect band gap of approximately 2.27 eV, with the maximum valence band occurring along the $\Gamma - X$ path at an energy of 1.19 eV and the minimum conduction band occurring along the $M - \Gamma$ path at an energy of 1.08 eV. To determine the contribution of carbon atoms with different hybridizations in the formation of electronic density of states, we plotted the partial density of states of the PG monolayer in panel 3(b). According to the figure, C_2 atoms with sp^2 hybridization have the highest contribution to the formation of electronic density of states, both in the valence and conduction bands. To obtain better and more realistic results, it is necessary to consider the intra-structure interactions. For this purpose, we apply the G_0W_0 approximation to account for electron-electron interactions. As shown in Fig. 4, the use of the G_0W_0 approximation leads to a wider band gap, which becomes quasi-direct with a value of 5.3 eV. This increase in the band gap is due to the self-energy corrections resulting from the electron-electron interactions. As shown in Table 1, the results extracted in this study are in good agreement with the results of the others.

Table 1: The values of the band gap are extracted from our calculations, which are compared with the similar results of the others.

Structure	Band gap: our results	Band gap: the others results
Penta-graphene monolayer	DFT-LDA: 2.25 eV	LDA: 2.22 eV [27]
	DFT-LDA: 2.32 eV	LDA: 2.27 eV [43]
	DFT-LDA: 5.53 eV	LDA: 4.48 eV [23]

3.3. Optical Properties

In calculations related to the optical properties of the selective structures, considering the ground state properties alone is not sufficient for interpreting or predicting the experimental results such as light propagation, absorption coefficient, loss coefficient, and the other optical parameters. Therefore, it is necessary to consider the effects of the excited states. To obtain the optical properties of a structure, the behavior of various optical quantities as a function of the incident photon energy needs to be studied.

Calculating the dielectric function $\varepsilon_M = \varepsilon_1 + i\varepsilon_2$ which includes both real and imaginary parts is a starting point for describing the optical properties of the structure. Here, the dielectric function is obtained by considering the local field effects (*LFE*), which are determined by the off-diagonal elements in the dielectric matrix. These effects strongly modify the total response to the light polarization of the external perturbation [39]. Our results show that the effects of the local fields on the calculated optical absorption spectra are negligible for parallel light polarization. It is shown that [40] the excitonic effects by considering the local-field effects in the optical absorption spectra of new type of hydrogenate graphene, finding that these local-field effects are highly important. Furthermore, LFEs, which can be vital for the light polarization perpendicular to the surface plane, are not neglected. It should be noted that the results related to the optical properties differ significantly between the cases of light polarization parallel and perpendicular to the plane. In the presence (absence) of the LFEs, Fig. 5 illustrates the absorption spectrum of a PG monolayer for two polarization states. The results indicate a significant difference in the absorption spectrum due to the application of LFEs for the polarization perpendicular to the plane compared to when these effects are not applied. When the LFEs are applied, the absorption spectrum is shifted towards higher energies (blue shift) and the absorption intensity is significantly reduced. On the other hand, in the case of light polarization parallel to the PG plane, significant variations in the absorption spectrum are not observed when we consider or neglect the LFEs. The similar results have been reported in the other structures [39]. Therefore, here, the light polarization parallel to the plane of PG is used. To obtain the dielectric function of PG, we first use the random phase approximation (RPA) based on the quasi-particle energy, where only the screened electron-electron interactions are considered (G_0W_0 -RPA approximation). Then, we use the Bethe-Salpeter equation approach based on the two-particle Green's function, where in addition to electron-electron interactions, electron-hole interactions are also considered (G_0W_0 -BSE). Fig. 6 shows the imaginary part and the real part of the dielectric function for PG monolayer in the presence of electron-hole interaction (G_0W_0 -BSE) and also in the absence of electron-hole interaction (G_0W_0 -RPA). As can be seen from panel (a) in Fig. 6,

the application of electron-hole interaction causes the absorption spectrum to shift towards lower energies (red shift) compared to the absorption spectrum obtained from the G_0W_0 -RPA approximation, and an important physical effect of this is the appearance of a number of bound excitons below the bandgap resulting from the GW approximation. The optical gap of PG, which is indicated by the first peak in the absorption spectrum and is consistent with the bound exciton, is 2.46 eV, and the binding energy of this exciton (defined as the difference between the quasi-particle bandgap and the exciton energy) is 3.07 eV. As shown in panel (b), the real part of the dielectric function is positive above zero energy when the G_0W_0 -RPA approximation is applied, but with the application of electron-hole interaction, its value becomes negative around 6 eV, indicating that no light is emitted in this energy range. The value of the real part of the dielectric function at zero energy is defined as the static dielectric constant, which was obtained as 1.41 eV for the G_0W_0 -RPA approximation and 1.52 eV for the G_0W_0 -BSE approximation, indicating an increase in the dielectric constant when using the G_0W_0 -BSE approximation compared to the G_0W_0 -RPA approximation, which has also been reported in other works [41]. In order to describe the other optical properties of the PG monolayer, the complex refractive index has been used, which is expressed by the following equation,

$$N(\omega) = n(\omega) + ik(\omega), \quad (2)$$

in which the real and imaginary parts represent the refractive index and the extinction coefficient, respectively. These two parts are calculated using the following equations [42],

$$\begin{aligned} n(\omega) &= \left(\frac{\sqrt{\varepsilon_1^2 \varepsilon_2^2 + \varepsilon_1}}{2} \right)^{\frac{1}{2}} \quad \text{and} \\ k(\omega) &= \left(\frac{\sqrt{\varepsilon_1^2 \varepsilon_2^2 - \varepsilon_1}}{2} \right)^{\frac{1}{2}}. \end{aligned} \quad (3)$$

Fig. 7 illustrates the calculated results for the refractive index and extinction coefficient of the PG monolayer in the presence (absence) of the electron-hole interaction. The refractive index at zero energy, known as the static refractive index, is introduced. According to panel (a) in Fig. 7, this value is 1.20 for the G_0W_0 -RPA approximation and 1.25 for the G_0W_0 -BSE approximation. Additionally, the maximum refractive index values for these two approximations are observed at 3.81 eV for the G_0W_0 -RPA approximation and 2.31 eV for the G_0W_0 -BSE approximation. In other studies [41], it has been observed that the static refractive index calculated using G_0W_0 -BSE is higher than the value obtained from G_0W_0 -RPA. Panel (b) in Fig. 7 shows the extinction coefficient of the PG monolayer, which demonstrates the electron-hole interactions cause a shift of the extinction coefficient plot towards lower energies (red shift). The maximum extinction coefficient for the G_0W_0 -RPA and G_0W_0 -BSE approximations is 0.70 and 0.99, respectively, which is observed at energies of 5.53 eV and 4.98 eV. At these energies, photons are rapidly absorbed. To proceed, the

reflectance is calculated using the following equation [43],

$$R(\omega) = \frac{(n - 1)^2 + k^2}{(n + 1)^2 + k^2}. \quad (4)$$

The reflectance spectrum, which represents the intensity of incident light reflection, is shown in Fig. 8. The maximum calculated reflectance value in the G_0W_0 -RPA approximation is observed at 8.71 eV with a value of approximately 14%. Similarly, for the G_0W_0 -BSE approximation, this value is approximately 19% at the energy of 6.35 eV. As evident from the Fig. 8, the application of electron-hole interactions leads to an increase in the maximum reflectance and a shift of the reflectance spectrum towards lower energies.

4. Conclusions and remarks

In conclusion, based on the presented methodology in section 2, we have investigated the electronic and optical properties of penta-graphene (PG) monolayer. The results at the DFT-GGA level indicate that PG is a semiconductor with an indirect band gap of approximately 2.32 eV. The utilization of the G0W0 approximation leads to an increase in the band gap, resulting in a quasi-direct gap of 5.35 eV. The GW band structure calculations showed that self-energy corrections were needed to obtain accurate quasi-particle properties for PG monolayer. Additionally, we have employed the G_0W_0 -RPA and G_0W_0 -BSE approximations to calculate the optical properties and investigate the variations in the different optical spectra in the presence and in the absence of electron-hole interactions. The results demonstrate that the inclusion of electron-hole interaction causes a red-shift of the absorption spectrum towards lower energies compared to the spectrum obtained from the G_0W_0 -RPA approximation. Because of the enhanced overlap between electrons and holes due to the low-dimensionality and the weak electronic screening effects in PG monolayer, optical absorption spectra were dominated by the first bound exciton with a significant binding energy, i.e., 3.07 eV. It is found that the PG monolayer, with a wider band gap and the enhanced excitonic effects, holds promise as a suitable candidate for the design and fabrication of electronic and optoelectronic components.

5. Acknowledgements

B.M., S.A.K. and J.M.S. acknowledges School of Physics, Damghan University. This work was supported in part by the Brazilian Agencies CAPES, CNPq, FAPESP and FAPEPI. J.M.S acknowledges CENAPAD-SP (Centro Nacional de Alto Desempenho em São Paulo - Universidade Estadual de Campinas - UNICAMP) provided computational support (proj842). J.M.S. acknowledges CNPq (Process No. 305053/2023 – 0) for financial support.

References

- [1] M. Dresselhaus, G. Dresselhaus, P. Eklund, Fullerenes, *Journal of materials research* 8 (8) (1993) 2054–2097.
- [2] L.-C. Qin, X. Zhao, K. Hirahara, Y. Miyamoto, Y. Ando, S. Iijima, The smallest carbon nanotube, *Nature* 408 (6808) (2000) 50–50.
- [3] Y. Li, L. Xu, H. Liu, Y. Li, Graphdiyne and graphyne: from theoretical predictions to practical construction, *Chemical Society Reviews* 43 (8) (2014) 2572–2586.
- [4] K. S. Novoselov, A. K. Geim, S. V. Morozov, D.-e. Jiang, Y. Zhang, S. V. Dubonos, I. V. Grigorieva, A. A. Firsov, Electric field effect in atomically thin carbon films, *science* 306 (5696) (2004) 666–669.
- [5] A. K. Geim, K. S. Novoselov, The rise of graphene, *Nature materials* 6 (3) (2007) 183–191.
- [6] A. K. Geim, Graphene: status and prospects, *science* 324 (5934) (2009) 1530–1534.
- [7] C. e. e. Rao, A. e. Sood, K. e. Subrahmanyam, A. Govindaraj, Graphene: the new two-dimensional nanomaterial, *Angewandte Chemie International Edition* 48 (42) (2009) 7752–7777.
- [8] Y. Zhu, S. Murali, W. Cai, X. Li, J. W. Suk, J. R. Potts, R. S. Ruoff, Graphene and graphene oxide: synthesis, properties, and applications, *Advanced materials* 22 (35) (2010) 3906–3924.
- [9] X. Du, I. Skachko, A. Barker, E. Y. Andrei, Approaching ballistic transport in suspended graphene, *Nature nanotechnology* 3 (8) (2008) 491–495.
- [10] A. A. Balandin, S. Ghosh, W. Bao, I. Calizo, D. Teweldebrhan, F. Miao, C. N. Lau, Superior thermal conductivity of single-layer graphene, *Nano letters* 8 (3) (2008) 902–907.
- [11] R. Grantab, V. B. Shenoy, R. S. Ruoff, Anomalous strength characteristics of tilt grain boundaries in graphene, *Science* 330 (6006) (2010) 946–948.
- [12] S. Sahu, G. Rout, Band gap opening in graphene: a short theoretical study, *International Nano Letters* 7 (2017) 81–89.
- [13] P. Silvestrelli, A. Ambrosetti, Bandgap opening in graphene using alkali ions by first principles, *Applied Physics Letters* 113 (21) (2018).
- [14] J.-S. Park, H. J. Choi, Band-gap opening in graphene: A reverse-engineering approach, *Physical Review B* 92 (4) (2015) 045402.
- [15] D. Q. Khoa, C. V. Nguyen, L. M. Bui, H. V. Phuc, B. D. Hoi, N. V. Hieu, V. Q. Nha, N. Huynh, L. C. Nhan, N. N. Hieu, Opening a band gap in graphene by c–c bond alternation: A tight binding approach, *Materials Research Express* 6 (4) (2019) 045605.
- [16] F. Ke, Y. Chen, K. Yin, J. Yan, H. Zhang, Z. Liu, J. S. Tse, J. Wu, H.-k. Mao, B. Chen, Large bandgap of pressurized trilayer graphene, *Proceedings of the National Academy of Sciences* 116 (19) (2019) 9186–9190.
- [17] H. Prinzbach, A. Weiler, P. Landenberger, F. Wahl, J. Wörth, L. T. Scott, M. Gelmont, D. Olevano, B. v. Issendorff, Gas-phase production and photoelectron spectroscopy of the smallest fullerene, c₂₀, *Nature* 407 (6800) (2000) 60–63.
- [18] S. Zhang, J. Zhou, Q. Wang, X. Chen, Y. Kawazoe, P. Jena, Penta-graphene: A new carbon allotrope, *Proceedings of the National Academy of Sciences* 112 (8) (2015) 2372–2377.
- [19] N. T. Tien, P. T. B. Thao, V. T. Phuc, R. Ahuja, Influence of edge termination on the electronic and transport properties of sawtooth penta-graphene nanoribbons, *Journal of physics and chemistry of solids* 146 (2020) 109528.
- [20] Z. G. Yu, Y.-W. Zhang, A comparative density functional study on electrical properties of layered penta-graphene, *Journal of Applied Physics* 118 (16) (2015).
- [21] X. Li, S. Zhang, F. Q. Wang, Y. Guo, J. Liu, Q. Wang, Tuning the electronic and mechanical properties of penta-graphene via hydrogenation and fluorination, *Physical Chemistry Chemical Physics* 18 (21) (2016) 14191–14197.
- [22] W. Xu, G. Zhang, B. Li, Thermal conductivity of penta-graphene from molecular dynamics study, *The Journal of chemical physics* 143 (15) (2015).
- [23] Z. Wang, F. Dong, B. Shen, R. Zhang, Y. Zheng, L. Chen, S. Wang, C. Wang, K. Ho, Y.-J. Fan, et al., Electronic and optical properties of novel carbon allotropes, *Carbon* 101 (2016) 77–85.

- [24] H. Sun, S. Mukherjee, C. V. Singh, Mechanical properties of monolayer penta-graphene and phagraphene: a first-principles study, *Physical Chemistry Chemical Physics* 18 (38) (2016) 26736–26742.
- [25] T. Stauber, J. I. Beltrán, J. Schliemann, Tight-binding approach to penta-graphene, *Scientific reports* 6 (1) (2016) 22672.
- [26] H.-J. Jia, H.-M. Mu, J.-P. Li, Y.-Z. Zhao, Y.-X. Wu, X.-C. Wang, Piezoelectric and polarized enhancement by hydrofluorination of penta-graphene, *Physical Chemistry Chemical Physics* 20 (41) (2018) 26288–26296.
- [27] H. Einollahzadeh, R. Dariani, S. Fazeli, Computing the band structure and energy gap of penta-graphene by using dft and g0w0 approximations, *Solid State Communications* 229 (2016) 1–4.
- [28] J. P. Perdew, K. Burke, M. Ernzerhof, Generalized gradient approximation made simple, *Physical review letters* 77 (18) (1996) 3865.
- [29] J. P. Perdew, K. Burke, Y. Wang, Erratum: Generalized gradient approximation for the exchange-correlation hole of a many-electron system [phys. rev. b 54, 16 533 (1996)], *Physical Review B* 57 (23) (1998) 14999.
- [30] J. P. Perdew, K. Burke, M. Ernzerhof, Perdew, burke, and ernzerhof reply, *Physical Review Letters* 80 (4) (1998) 891.
- [31] N. Troullier, J. L. Martins, Efficient pseudopotentials for plane-wave calculations, *Physical review B* 43 (3) (1991) 1993.
- [32] W. G. Aulbur, L. Jönsson, J. W. Wilkins, Quasiparticle calculations in solids, *Solid state physics* (New York. 1955) 54 (2000) 1–218.
- [33] S. Korbil, P. Boulanger, I. Duchemin, X. Blase, M. A. Marques, S. Botti, Benchmark many-body gw and bethe–salpeter calculations for small transition metal molecules, *Journal of chemical theory and computation* 10 (9) (2014) 3934–3943.
- [34] L. Hedin, B. I. Lundqvist, Explicit local exchange-correlation potentials, *Journal of Physics C: Solid state physics* 4 (14) (1971) 2064.
- [35] R. W. Godby, R. Needs, Metal-insulator transition in kohn-sham theory and quasiparticle theory, *Physical review letters* 62 (10) (1989) 1169.
- [36] G. Onida, L. Reining, A. Rubio, Electronic excitations: density-functional versus many-body green’s-function approaches, *Reviews of modern physics* 74 (2) (2002) 601.
- [37] M. Rohlfing, S. G. Louie, Electron-hole excitations and optical spectra from first principles, *Physical Review B* 62 (8) (2000) 4927.
- [38] A. Marini, C. Hogan, M. Grüning, D. Varsano, Yambo: an ab initio tool for excited state calculations, *Computer Physics Communications* 180 (8) (2009) 1392–1403.
- [39] M. Ashhadi, S. A. Ketabi, Quasi-particle energies and excitonic effects in bilayer of hexagonal boron nitride, *Solid state communications* 187 (2014) 1–4.
- [40] W. Wei, T. Jacob, Strong charge-transfer excitonic effects in c 4 h-type hydrogenated graphene, *Physical Review B* 86 (16) (2012) 165444.
- [41] M. Shahrokhi, Quasi-particle energies and optical excitations of zns monolayer honeycomb structure, *Applied Surface Science* 390 (2016) 377–384.
- [42] A. Ghojavand, S. J. Hashemifar, M. Tarighi Ahmadpour, A. V. Shapeev, A. Alhaji, Q. Hassanzada, Ab initio analysis of structural and electronic properties and excitonic optical responses of eight ge-based 2d materials, *Journal of Applied Physics* 127 (21) (2020).
- [43] G. R. Berdiyrov, M. E.-A. Madjet, First-principles study of electronic transport and optical properties of penta-graphene, penta-sic 2 and penta-cn 2, *RSC advances* 6 (56) (2016) 50867–50873.

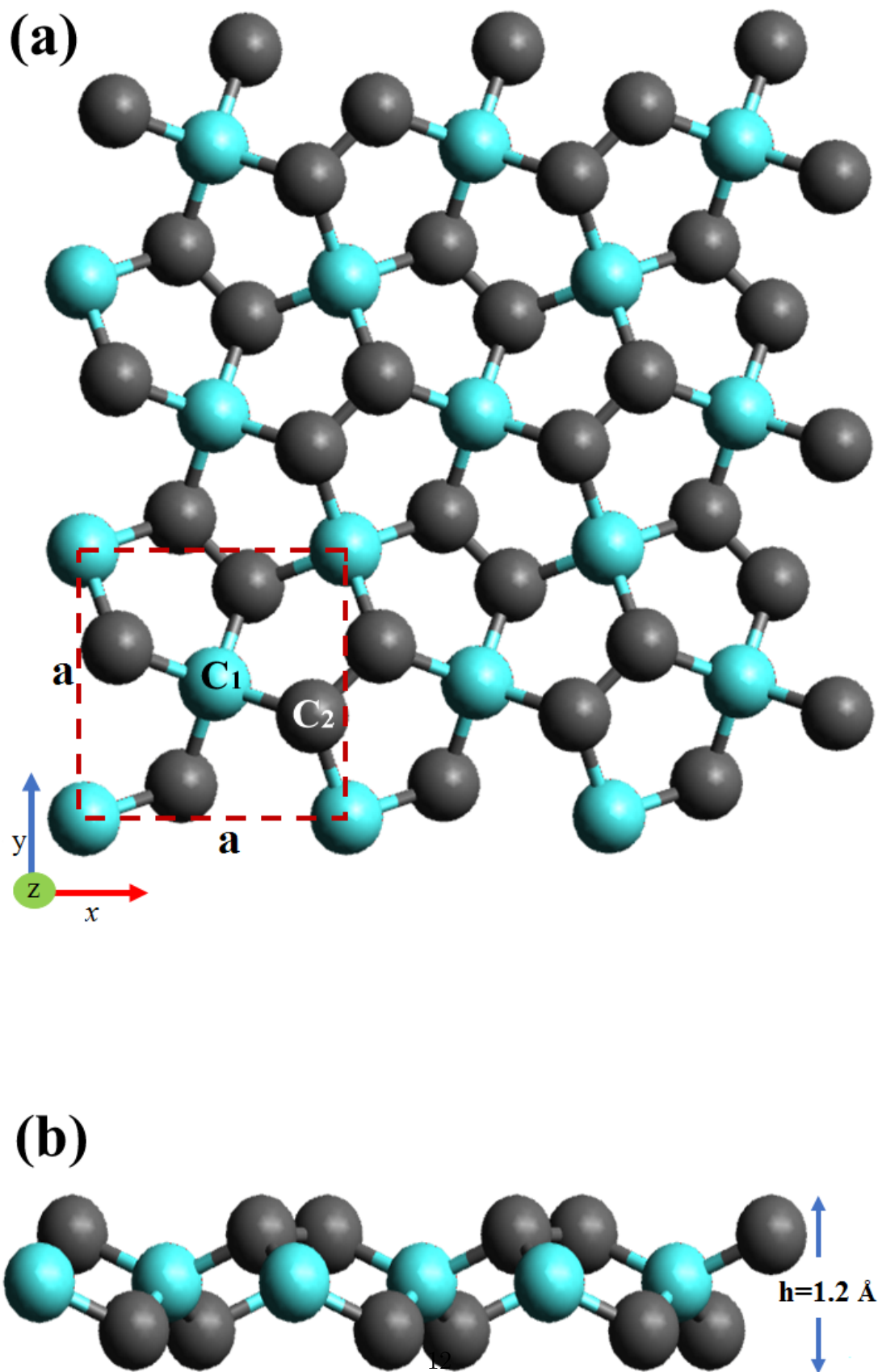


Figure 1: (Colour online) The plot shows schematically penta-graphene (PG) monolayer structure. (a) top view and (b) side view. The square shown with dashed red lines is the primitive unit cell of PG.

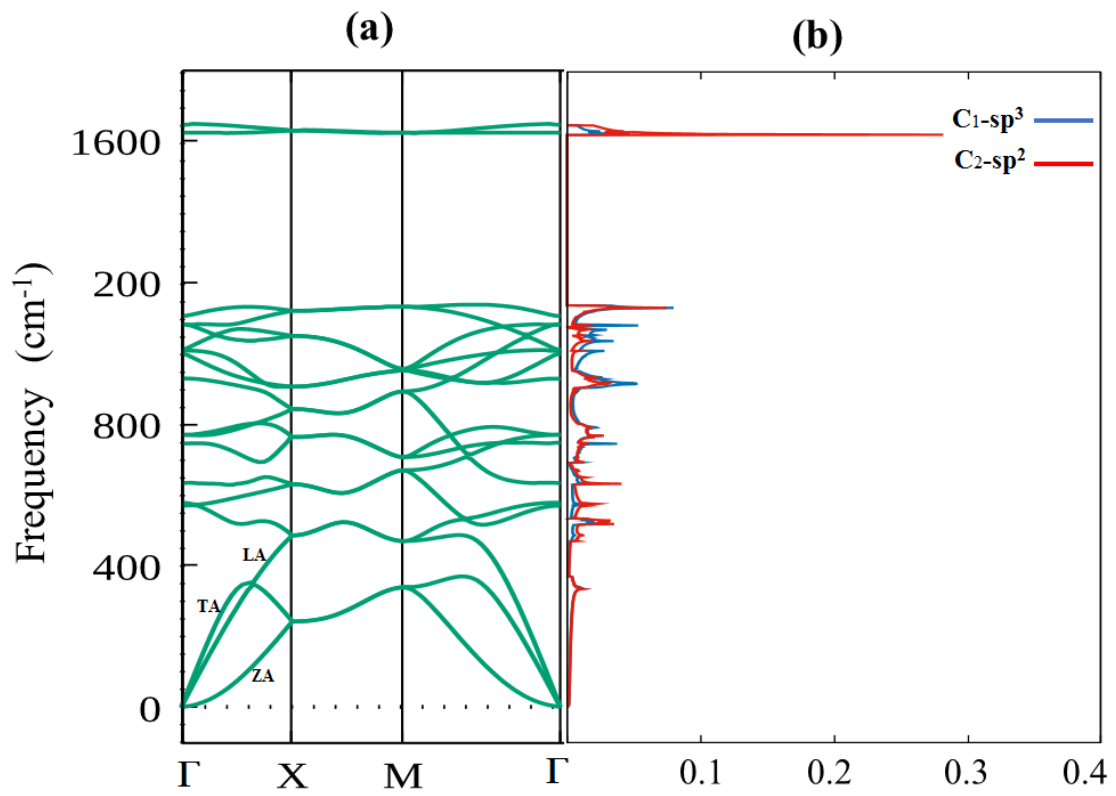


Figure 2: (Colour online) Panels (a) and (b) show phonon spectra and phonon density of states of the PG monolayer, respectively.

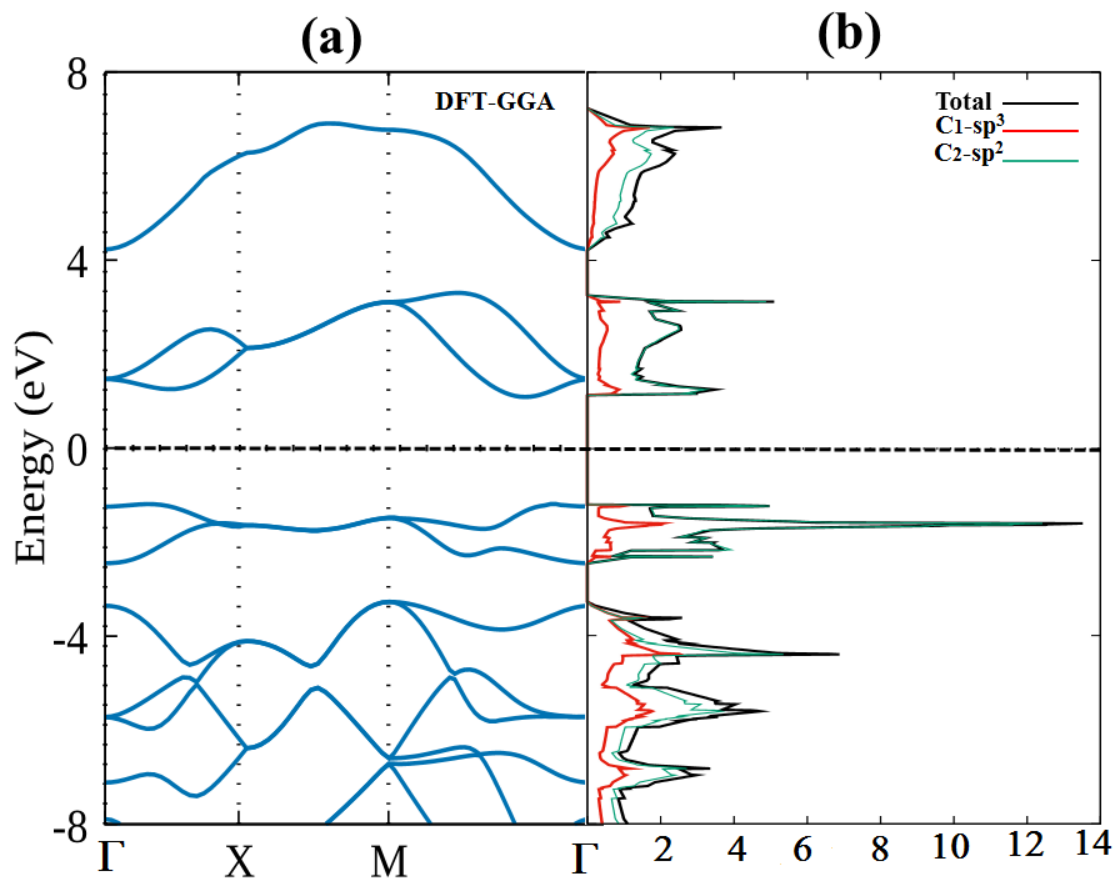


Figure 3: (Colour online) Panels (a) and (b) show the electronic band structure and density of partial states of PG monolayer, respectively calculated with GGA-PBE functional. Fermi level is considered at zero point.

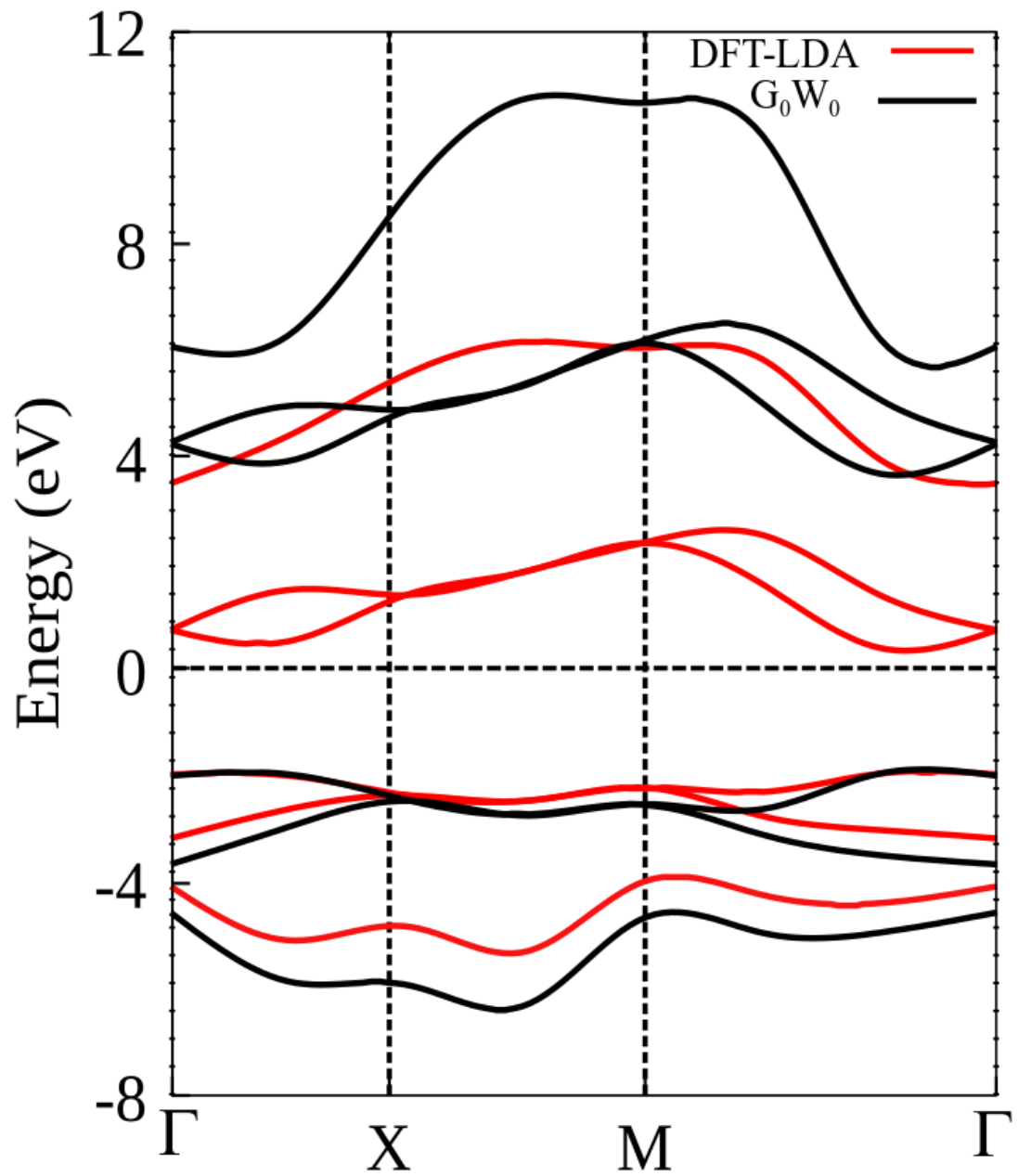


Figure 4: (Colour online) Plot shows the PG electronic band structure calculated by DFT-LDA (red curve) and G_0W_0 (black curve).

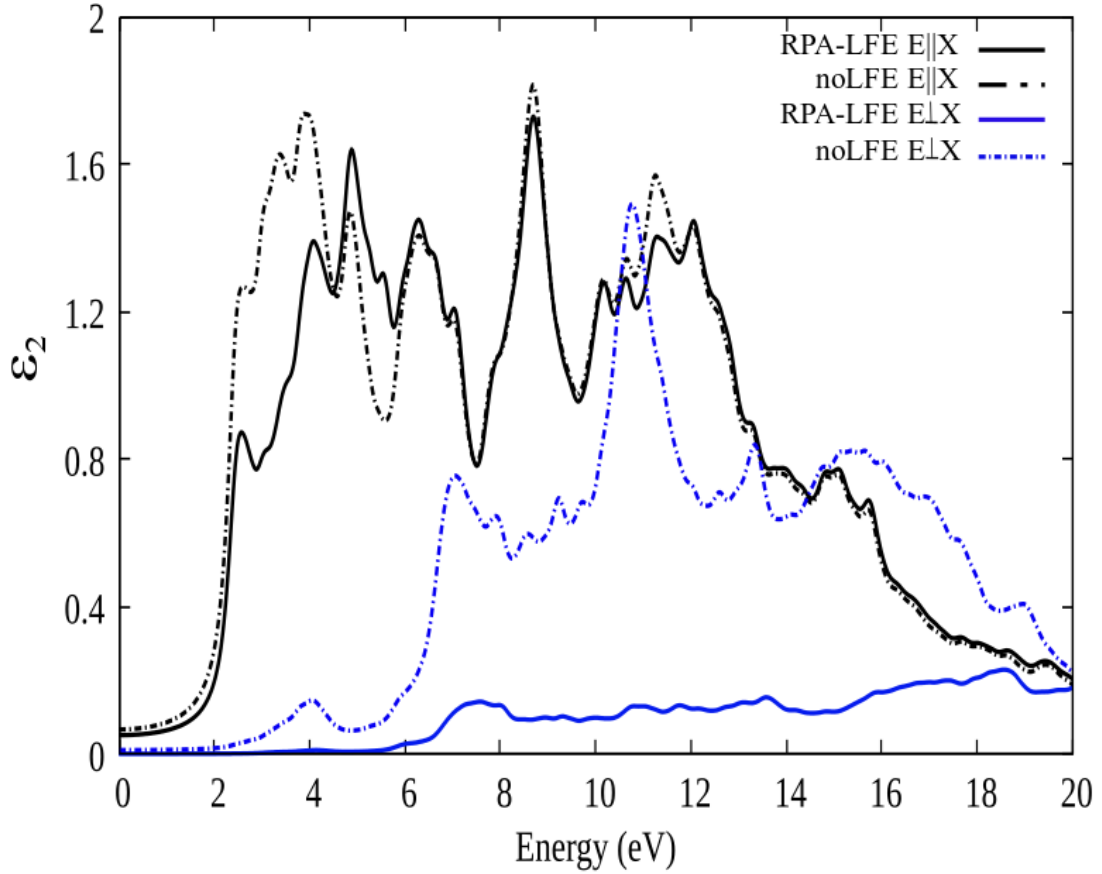


Figure 5: (Colour online) Plot shows the imaginary part of the dielectric function of the PG monolayer. Taking into account the LFE, black solid curve illustrates the polarization of light parallel to the PG plane. The dash-dotted black curve shows the same situation without LFE. Taking into account the LFE, blue solid curve illustrates the polarization of light perpendicular to the PG plane. The dash-dotted blue curve shows the same situation without LFE.

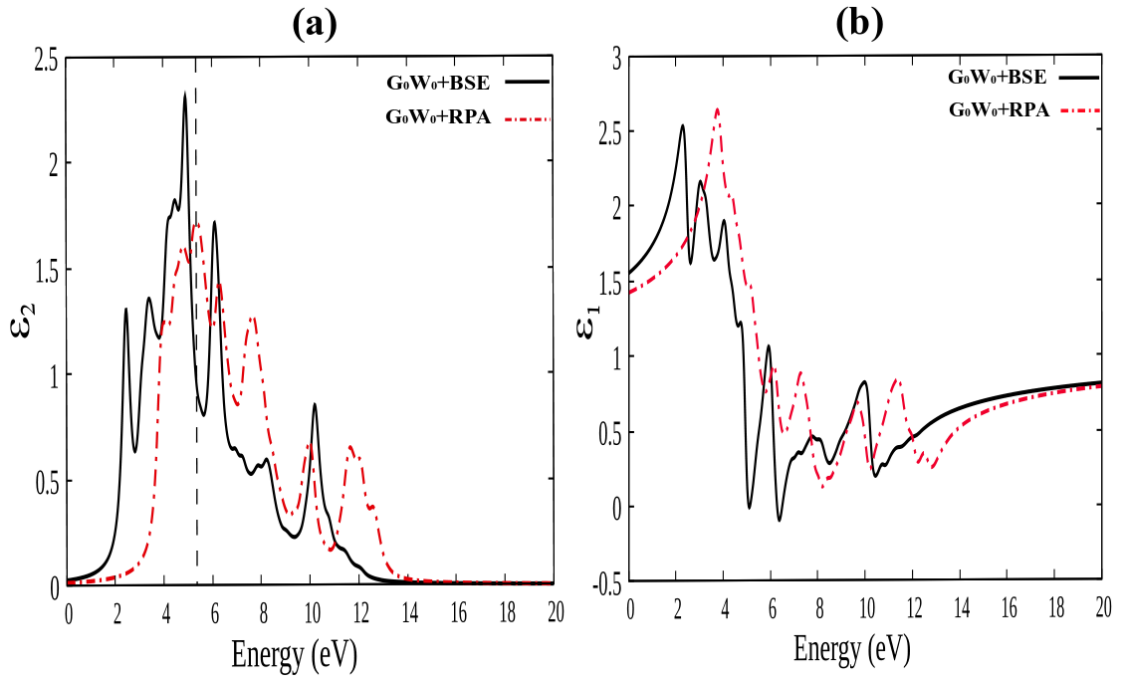


Figure 6: (Colour online) Panels (a) and (b) illustrate the imaginary and real parts of the dielectric function of PG monolayer, respectively for the light polarization parallel to the PG plane ($E//X$) in the presence (black curve) and in the absence (dash-dotted red curve) of the electron-hole interaction. From zero energy to the vertical dotted line in the imaginary part shows the size of band gap resulting from G₀W₀ approximation.

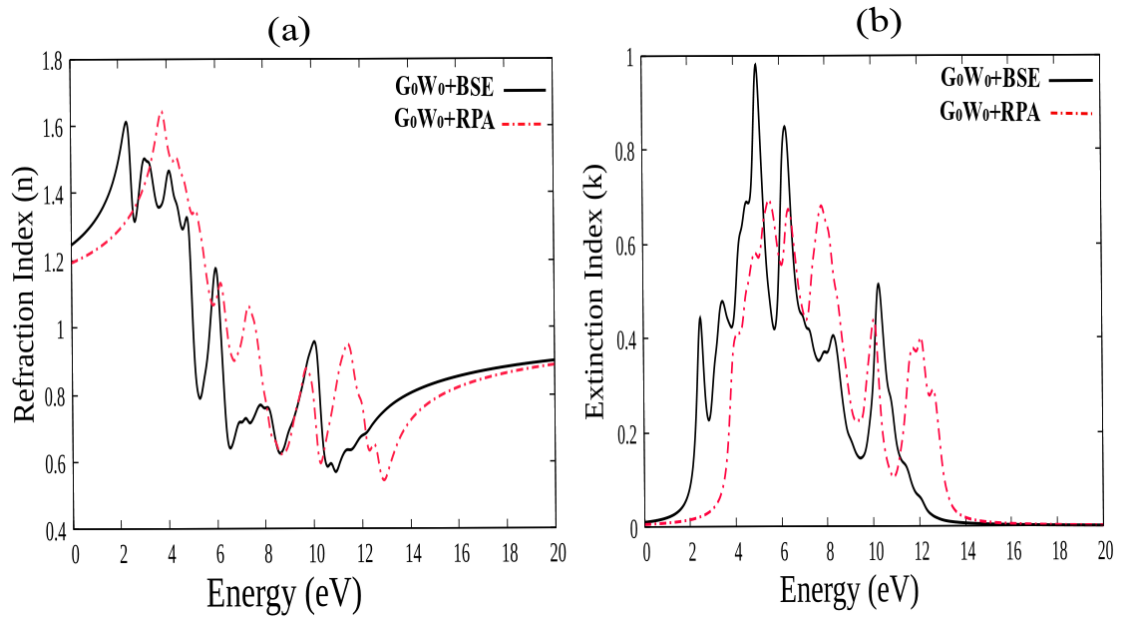


Figure 7: (Colour online) Panels (a) and (b) illustrate the refractive index n and the extinction coefficient k of the PG monolayer, respectively in the presence (black curve) and in the absence (dash-dotted red curve) of the electron-hole interaction.

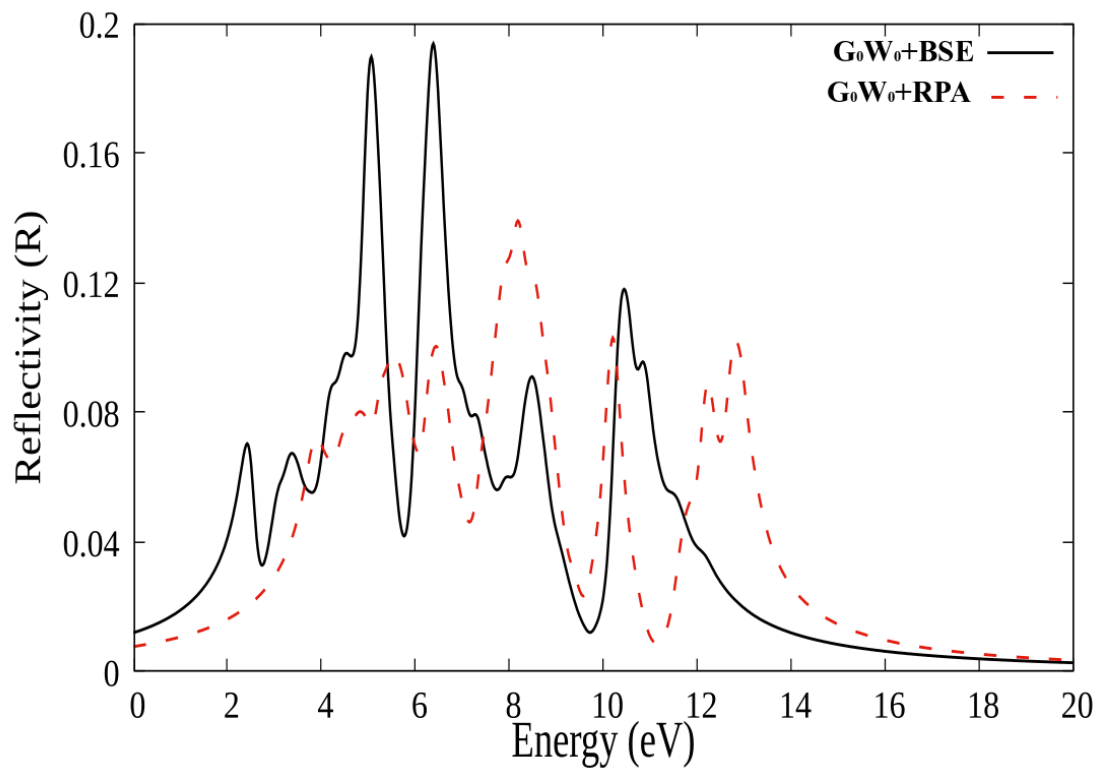


Figure 8: (Colour online) Plot shows the reflection spectra of the PG monolayer in the presence (black curve) and in the absence (dash-dotted red curve) of the electron-hole interaction.